2

POR-2059(EX)
(WT-2059)(EX)
EXTRACTED VERSION

OPERATION DOMINIC, FISH BOWL SERIES

Project Officer's Report—Project 7.2b

Microwave Radiometric Measurements

D. M. Towle, Project Officer
M. Balser
J. J. Kirwan
J. H. Pannell
Lincoln Laboratory
Lexington, MA

31 December 1964

NOTICE:
This is an extract of POR-2059 (WT-2059), Operation DOMINIC, Fish Bowl Series, Project 7.2b.

Extracted version prepared for
Director
DEFENSE NUCLEAR AGENCY
Washington, DC 20305-1000

1 September 1985

UNCLASSIFIED
SECURITY CLASSIFICATION OF THIS PAGE

AD-A995 429

REPORT DOCUMENTATION PAGE

1a. REPORT SECURITY CLASSIFICATION UNCLASSIFIED	1b. RESTRICTIVE MARKINGS
2a. SECURITY CLASSIFICATION AUTHORITY	3. DISTRIBUTION/AVAILABILITY OF REPORT Approved for public release; distribution is unlimited.
2b. DECLASSIFICATION/DOWNGRADING SCHEDULE	
4. PERFORMING ORGANIZATION REPORT NUMBER(S)	5. MONITORING ORGANIZATION REPORT NUMBER(S) POR-2059 (EX) (WT-2059) (EX)
6a. NAME OF PERFORMING ORGANIZATION Lincoln Laboratory 6b. OFFICE SYMBOL (If applicable)	7a. NAME OF MONITORING ORGANIZATION Defense Atomic Support Agency
6c. ADDRESS (City, State, and ZIP Code) Lexington, MA	7b. ADDRESS (City, State, and ZIP Code) Washington, DC
8a. NAME OF FUNDING/SPONSORING ORGANIZATION 8b. OFFICE SYMBOL (If applicable)	9. PROCUREMENT INSTRUMENT IDENTIFICATION NUMBER
8c. ADDRESS (City, State, and ZIP Code)	10. SOURCE OF FUNDING NUMBERS PROGRAM ELEMENT NO. | PROJECT NO. | TASK NO. | WORK UNIT ACCESSION NO.

11. TITLE (Include Security Classification) OPERATION DOMINIC; FISH BOWL SERIES, PROJECT OFFICER'S REPORT; PROJECT 7.2b - Microwave Radiometric Measurements, Extracted Version

12. PERSONAL AUTHOR(S)
D. M. Towle, M. Balser, J. J. Kirwan, and J. H. Pannell

13a. TYPE OF REPORT	13b. TIME COVERED FROM ___ TO ___	14. DATE OF REPORT (Year, Month, Day)	15. PAGE COUNT
		1964, December 31	86

16. SUPPLEMENTARY NOTATION This report has had sensitive military information removed in order to provide an unclassified version for unlimited distribution. The work was performed by the Defense Nuclear Agency in support of the DoD Nuclear Test Personnel Review Program.

17. COSATI CODES

FIELD	GROUP	SUB-GROUP
18	3	
20	14	

18. SUBJECT TERMS (Continue on reverse if necessary and identify by block number)
Dominic, Microwaves, Check Mate, Fish Bowl, Star Fish Prime, King Fish, Radiometric Measurements, Blue Gill Triple Prime

19. ABSTRACT (Continue on reverse if necessary and identify by block number)
The electromagnetic energy incident on ground-based antennas on Johnston Island as a result of the five high-altitude nuclear bursts of the Fish Bowl series was measured in the frequency regions around 925 Mc, 3000 Mc, and 24,500 Mc by the radiometric techniques described in this report. The data, recorded in terms of antenna temperatures, are directly interpretable as physical temperatures of the thermally radiating regions and allow the deduction of the attenuation encountered by radio-frequency signals passing through the burst regions.

The time history of the temperatures of the burst region for the three microwave frequencies of the radiometric measurements presented considerable insight into the physical processes occurring during the high-altitude events. Electron densities and recombination rates have been deduced from the radiometric data.

20. DISTRIBUTION/AVAILABILITY OF ABSTRACT ☒ UNCLASSIFIED/UNLIMITED ☐ SAME AS RPT. ☐ DTIC USERS	21. ABSTRACT SECURITY CLASSIFICATION UNCLASSIFIED
22a. NAME OF RESPONSIBLE INDIVIDUAL MARK D. FLOHR	22b. TELEPHONE (Include Area Code) 202-325-7559 22c. OFFICE SYMBOL DNA/ISCM

DD FORM 1473, 84 MAR

83 APR edition may be used until exhausted.
All other editions are obsolete.

SECURITY CLASSIFICATION OF THIS PAGE
UNCLASSIFIED

OPERATION DOMINIC

FISH BOWL SERIES

PROJECT OFFICERS REPORT—PROJECT 7.2b

MICROWAVE RADIOMETRIC MEASUREMENTS

D.M. Towle, Project Officer
M. Balser
J.J. Kirwan
J.H. Pannell

Lincoln Laboratory
Lexington, Massachusetts

DEPARTMENT OF DEFENSE
WASHINGTON, D.C. 20301

FOREWORD

Classified material has been removed in order to make the information available on an unclassified, open publication basis, to any interested parties. The effort to declassify this report has been accomplished specifically to support the Department of Defense Nuclear Test Personnel Review (NTPR) Program. The objective is to facilitate studies of the low levels of radiation received by some individuals during the atmospheric nuclear test program by making as much information as possible available to all interested parties.

The material which has been deleted is either currently classified as Restricted Data or Formerly Restricted Data under the provisions of the Atomic Energy Act of 1954 (as amended), or is National Security Information, or has been determined to be critical military information which could reveal system or equipment vulnerabilities and is, therefore, not appropriate for open publication.

The Defense Nuclear Agency (DNA) believes that though all classified material has been deleted, the report accurately portrays the contents of the original. DNA also believes that the deleted material is of little or no significance to studies into the amounts, or types, of radiation received by any individuals during the atmospheric nuclear test program.

ABSTRACT

The electromagnetic energy incident on ground-based antennas on Johnston Island as a result of the five high-altitude nuclear bursts of the Fish Bowl series was measured in the frequency regions around 925 Mc, 3000 Mc, and 34,500 Mc by the radiometric techniques described in this report. The data, recorded in terms of antenna temperatures, are directly interpretable as physical temperatures of the thermally radiating regions and allow the deduction of the attenuation encountered by radio-frequency signals passing through the burst regions.

The peak microwave temperatures were found to decrease with altitude

The fireball region of all shots was found to attenuate 34,500-Mc signals severely for several seconds and 3000-Mc signals for several minutes.

The one-way attenuation on a radial path to the Blue Gill fireball was calculated to be 10 db for 34,500 Mc at one second; for Tight Rope, it was 13 db for 34,500 Mc at one-half second. The attenuation through the Star Fish burst region was demonstrated to be unimportant for microwave signals in the frequency region of 3000 Mc and above.

The noise, which would be injected into a radar receiver by high-altitude bursts, can be calculated directly from the radiometric data obtained. A radar system with a narrow beamwidth pointed directly at a nuclear burst

This situation rigorously restricts the ultimate sensitivity which can be achieved by the use of low-noise receivers for radars to be operated in such an

environment. The effectiveness of a nuclear burst as a generator of microwave noise increases with altitude

The time history of the temperatures of the burst region for the three microwave frequencies of the radiometric measurements presented considerable insight into the physical processes occurring during the high-altitude events. Electron densities and recombination rates have been deduced from the radiometric data.

PREFACE

The authors of this report are deeply indebted to many individuals from Lincoln Laboratory and from other agencies for their contributions to the project. L. Cartledge, J. McGinn, D. Griffin, A. Radys, and R. Williams served the project unstintingly both in the field and in the Laboratory.

Special thanks are due to Marion Schuler of Edgerton, Germeshausen and Grier, Inc., who provided much of the information presented in Tables 3.2, 3.3, and 3.4 of this report.

Suggestions and comments by J. Perry have added materially to the report.

The project also owes a debt to J. Freedman and G. Watson for support and encouragement during the project and to J. Meyer, without whose foresight and understanding, the project could not have been undertaken.

CONTENTS

TABLES

FIGURES

CHAPTER 1

INTRODUCTION

1.1 OBJECTIVES

The primary objective of Lincoln Laboratory's Project 7.2b during the Fish Bowl Series was to measure the electromagnetic energy incident on ground-based antennas on Johnston Island as a result of the high-altitude nuclear bursts in the frequency regions around 925 Mc (hereafter, L-band), 3000 Mc (S-band), and 34,450 Mc (K_a-band).

Five high-altitude tests were conducted during the series. These are summarized briefly in Table 1.1.

Quantitative data were obtained in all five of these tests. The data recorded in terms of antenna temperatures are directly interpretable as physical temperatures of the thermally radiating regions and allow the deduction of the attenuation encountered by radio-frequency signals passing through the burst region.

1.2 BACKGROUND AND THEORY

Thermal radiation is the result of energy exchange of charged particles caused by random interactions. These may take the form, for example, of transitions of state of bound electrons resulting from collisions with other particles. In the situation of interest to this investigation, the ionized particles in the plasma generated by the nuclear burst interact with each other and with electromagnetic radiation in a free-free type transition. This bremsstrahlung results in a much broader spectrum than that of the well-known synchrotron radiation generated by the interaction of the charged particles with the magnetic field. The primary microscopic mechanism in the generation and absorption of the microwave radiation investigated by the radiometric measurements reported here is this free-free type transition occurring among the charged particles produced by the nuclear burst.

For the case of a body in thermal equilibrium which absorbs all incident radiation, the radiated spectrum is a universal function of frequency characterized by the temperature T. The intensity of radiation and the complete spectrum for such a black body is given in terms of the temperature by the Planck radiation law. Other bodies may, for a variety of reasons, radiate an entirely different spectrum. The radiation at a given frequency may still be characterized by the temperature of the black body which would radiate an equal amount at that frequency. The electromagnetic energy received by an antenna is ultimately absorbed in a matched resistive load. The signal power available at the input of the amplifier from this termination is

$$P = k\, T_A\, B \tag{1.1}$$

where k is Boltzmann's constant, T_A is the effective antenna temperature, and B is the bandwidth. For an antenna enclosed in a black body of temperature T_M, it can be shown by use of Planck's radiation law that the intuitive result, $T_A = T_M$, is valid.

It is useful to consider the situation depicted below. Radiation characterized by the radiation temperature T_S passes through an attenuating layer before reaching the antenna.

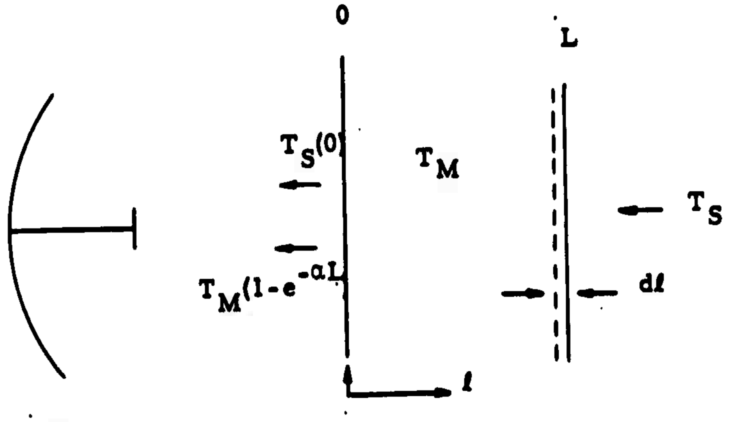

If the absorption coefficient of the medium is $\alpha(\ell)$, the signal is decreased by an amount

$$dT = -\alpha(\ell)\, T_S\, d\ell \tag{1.2}$$

in traversing a vanishingly thin layer $d\ell$. For a uniform layer of thickness, L, this may be integrated to give

$$T_S(0) = T_S e^{-\alpha L} \tag{1.3}$$

where $T_S(0)$ represents the remaining signal at the antenna. In the hypothetical case for which the medium is semi-infinite in extent, the antenna temperature must equal the medium temperature T_M. Therefore, the radiation temperature which originates in the layer of thickness, L, is

$$T_M(0) = T_M\,(1 - e^{-\alpha L}) \tag{1.4}$$

and the total antenna temperature is then

$$T_A = T_S e^{-\alpha L} + T_M\,(1 - e^{-\alpha L}) \tag{1.5}$$

The factor $e^{-\alpha L}$ is the transmittance of the layer, more simply designated as τ_m. The behavior of the antenna temperature may be inferred from this relation. If the attenuation is small, i.e., $\alpha L \to 0$, the antenna sees the background temperature T_S. If the attenuation of the layer is large, i.e., $\alpha L >> 1$, the antenna temperature approaches the temperature of the layer, and the contribution from the source T_S becomes negligible.

For the purpose of interpreting a typical situation, the temperature T_S may be considered to represent the sky background signal and T_M a layer formed by the burst either in the fireball itself or in the ionized atmosphere. At low radio frequencies (i.e., less than a hundred megacycles per second), the sky background temperature T_S is many thousand degrees (Kelvin). The objective of a well-known series of measurements (Reference 1), which was carried out with riometers distributed over a wide area, was, in fact, to monitor $T_S e^{-\alpha L}$ and thereby determine the increase in the atmospheric attenuation in the frequency region 20 Mc to 120 Mc following a high-altitude nuclear blast.

At the higher microwave frequencies at which the radiometers of this project were operated, the sky background temperature T_S becomes quite small (e.g., 20°K at L-band and 1° K at K_a-band) and, as a general rule, does not contribute appreciably to the antenna temperatures. During these measurements, the antennas were directed toward the fireball, and this was the principal source of radiation and absorption, while the intervening atmosphere was another potentially absorbing layer. The appropriate form of the antenna temperature relation in this situation is then

$$T_A = \tau_M T_B(1 - \tau_B) + T_M(1 - \tau_M) + T_S \tau_M \tau_B \qquad (1.6)$$

where T_B is the temperature of the burst region and τ_B its transmittance.

It is of interest now to consider what result would be obtained as a function of frequency under the assumption that the electron density is considerably higher than that in the intervening atmosphere. For the sake of simplifying the discussion, it is also assumed that the temperatures T_A and T_B are independent of frequency. At very low frequencies, radiation is absorbed in the lower layer ($\tau_M = 0$), and the antenna would see the layer temperature T_M. For higher frequencies, the lower layer becomes transparent ($\tau_M \rightarrow 1$) while the second region remains opaque ($\tau_B = 0$), and the antenna would see the temperature of the burst region T_B. For still higher frequencies (or lower electron densities), the burst region becomes transparent ($\tau_B \rightarrow 0$), and the antenna would see through the burst region. Examples of each of these conditions will be found in the results. The second condition above, for which the antenna temperature becomes approximately equal to the temperature of the burst region, occurs often enough in practice to make the radiometric measurements a valuable method of determining the temperature of the burst region directly from the observations. The more observing frequencies that are used, the better the individual quantities T_B, τ_B, and τ_M can be determined directly from the measurements. In some instances, additional independent data, for example, optical estimates of T_B, are necessary to determine the τ_B, or the absorption, explicitly from the radiometry data.

The attenuation in decibels, $L_M = 10 \log \frac{1}{\tau_M}$, of electromagnetic radiation in an ionized medium may be related to the electron-ion density by some of the relations found in plasma theory (Reference 2).

Thus,

$$L_M = 4.6 \times 10^{-2} \int \frac{n_e \, \nu \, dl}{4\pi^2 f^2 + \nu^2} \qquad (1.7)$$

where n_e is the electron density, cm^{-3}, ν is the electron collision frequency, and f is the frequency of the electromagnetic radiation in megacycles per second. Introducing the expression for ν for a fully ionized plasma and assuming a uniform layer of thickness L (in kilometers), the expression for the attenuation becomes

$$L_M \approx \frac{2 \times 10^{-8}\, n_e^2\, L}{f^2\, T^{3/2}} \tag{1.8}$$

where the appropriate condition $4\pi^2 f^2 >> \nu^2$ has been applied. This relation is useful in making rough comparisons of the radiometric results with the physical conditions to the extent that they are known.

Aside from the above considerations, the use of high microwave frequencies in this type of observation has the obvious advantage that highly directive beams may be formed with relatively small antennas. The burst area itself or nearby localized areas may then be probed independently with increased sensitivity by the finer beamwidths.

It is necessary even in the case of narrow beamwidths to consider the effect of the finite size of the beam on the measurements. In general, the burst region does not fill the beam completely, and the antenna temperature is proportionately smaller than the source temperature, i. e.,

$$T_A = f_A\, T_B \tag{1.9}$$

where f_A is a beam-filling factor. (It is assumed for the moment that the transmittance of the source is zero ($\tau_B = 0$).) If the antenna beam were a single conical-shaped lobe of constant gain throughout the solid angle Ω_A with zero gain elsewhere, and the source of uniform temperature throughout the solid angle Ω_B which lies within Ω_A, the filling factor would be

$$f_A = \frac{\Omega_B}{\Omega_A} \qquad \text{for } \Omega_B < \Omega_A$$

$$f_A = 1 \qquad \text{for } \Omega_B \geq \Omega_A \tag{1.10}$$

For a real antenna, however, the gain is not constant throughout the main lobe, and some energy enters the antenna by way of its unavoidable sidelobes. The gain patterns of the radiometric antennas at K_a-band, S-band, and L-band are shown in cross section in Figs. 1.1, 1.2, and 1.3, respectively. The antenna temperature is then an average of the source temperature weighted by the antenna gain function and is given by

$$T_A = \frac{\iint\limits_{\Omega_B} T_B(\Omega)\, G(\Omega)\, d\Omega}{\iint\limits_{4\pi} G(\Omega)\, d\Omega} \qquad (1.11)$$

where Ω_B is the solid angle subtended by the source at the antenna, and $G(\Omega)$ is the gain function of the antenna. In general, it is not possible to find a complete solution of Equation 1.11 even for an idealized case in which $G(\Omega)$ is represented by an analytic function. However, it is useful to consider the special case in which a uniform source of circular cross section is centered in the direction of maximum gain of the antenna. In polar coordinates

$$T_A = f_A\, T_B$$

where

$$f_A = \frac{\int_0^{2\pi}\int_0^{\phi_B} G(\phi, \varphi) \sin\phi \, d\phi \, d\varphi}{\int_0^{2\pi}\int_0^{\pi} G(\phi, \varphi) \sin\phi \, d\phi \, d\varphi} \qquad (1.12)$$

This integral has been evaluated numerically for the three radiometric antennas used in this project under the conditions stated. These results are presented in Figs. 1.4, 1.5, and 1.6 for the K_a-band, the S-band, and the L-band antennas, respectively, and are utilized extensively in the interpretation of the data. One over-simplified conclusion to be noted is that for K_a-band, $f_A \approx 0.9$ during most of the time for each event, and at S-band $f_A \approx 0.8$ during much of the measurement period of the three highest shots.

The role of several parameters which affect the measurements in an incidental manner have not yet been discussed. The antenna signals were measured at the input of the radiometer after passing through a length of transmission line. These line losses were measured and appropriate corrections applied to the measured signals to obtain the antenna signals. At K_a-band the water vapor and the oxygen in the atmosphere attenuate the signal a small amount before it reaches the antenna. This loss ($e^{\alpha_M L_M}$) is a function of the local weather conditions and must be measured shortly before the nuclear event. This was accomplished by noting the change in antenna temperature as a function of the elevation angle by a method introduced by Dicke (Reference 3). The contribution of the sky temperature T_S was estimated from a measurement of the total antenna temperature in those cases for which it conceivably might be appreciable. The total signal temperature at the radiometer prior to shot time is

$$T_R = T_S \tau_M \tau_L + T_M(1 - \tau_M) \tau_L + T_L(1 - \tau_L) + 2\pi \varepsilon T_G \bar{G} \quad (1.13)$$

where T_R is the resultant signal including the plumbing loss, τ_L is the transmittance of the transmission line (τ_L = 1/line loss), and the term $2\pi \varepsilon T_G \bar{G}$, in which T_G is the ground temperature, ε its emissivity, and $\bar{G}$ the average gain of the sidelobes subtending the ground, represents a small, nearly constant contribution to the total antenna temperature from the sidelobes which intercept the ground. Measurement of the total antenna temperature at the input to the radiometer, prior to the nuclear event, provides a valuable check not only on the atmospheric loss but also on any change in the transmission line losses which sometimes occurs in a tropical climate where moisture is prevalent.

The results which are given in the following sections are presented in terms of the increase in antenna temperature over its quiescent value prior to the nuclear event and represent the contribution to the total antenna temperature due to the nuclear effects. Corrections have been made for the various systematic losses.

TABLE 1.1 SUMMARY OF EVENTS

Event	Date	Altitude km	Yield
Star Fish Prime	July 9, 1962	400	1.3 Mt
Check Mate	Oct. 20, 1962		
King Fish	Nov. 1, 1962		
Blue Gill Triple Prime	Oct. 26, 1962		
Tight Rope	Nov. 4, 1962		

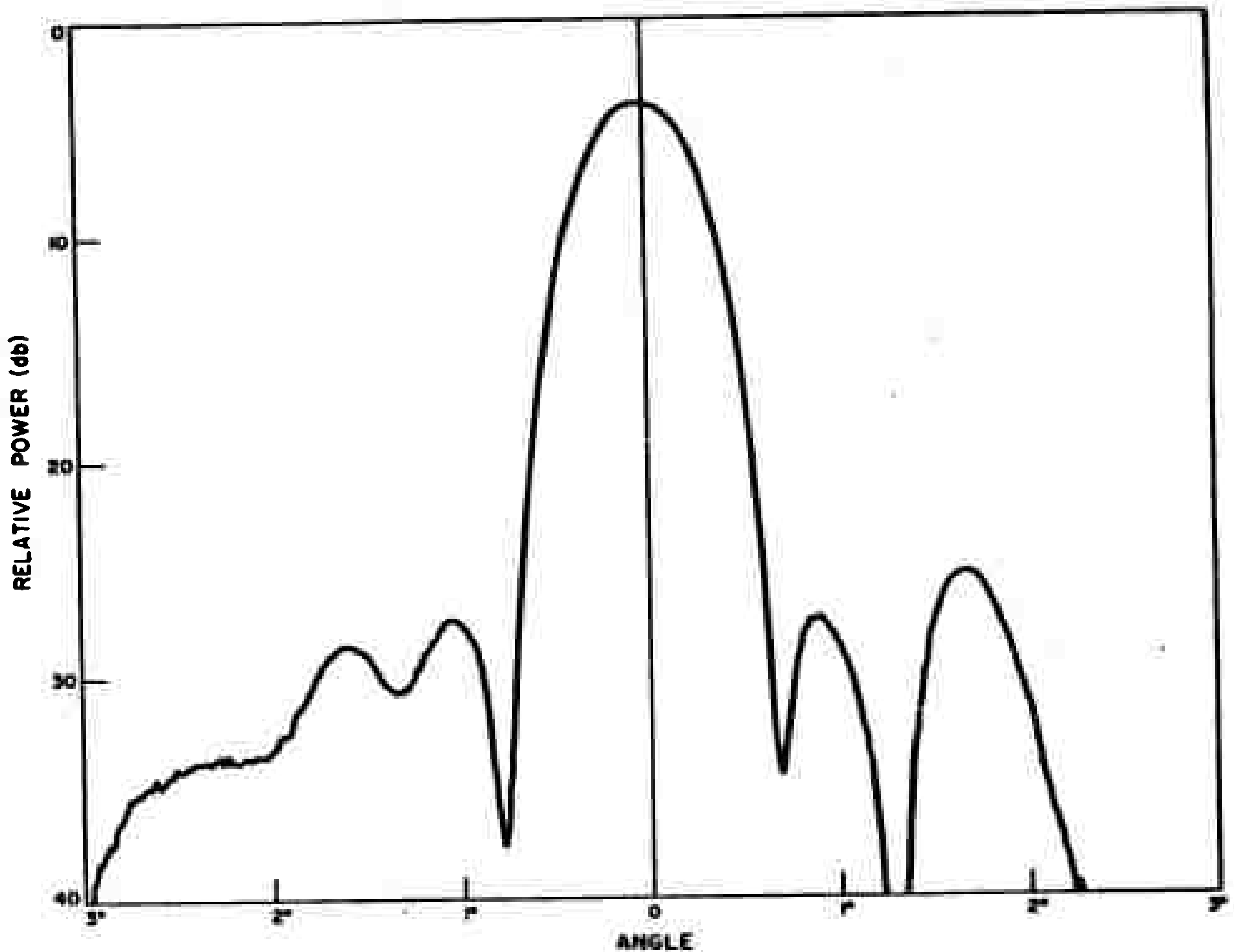

Figure 1.1 K_a-band antenna pattern. E-plane.

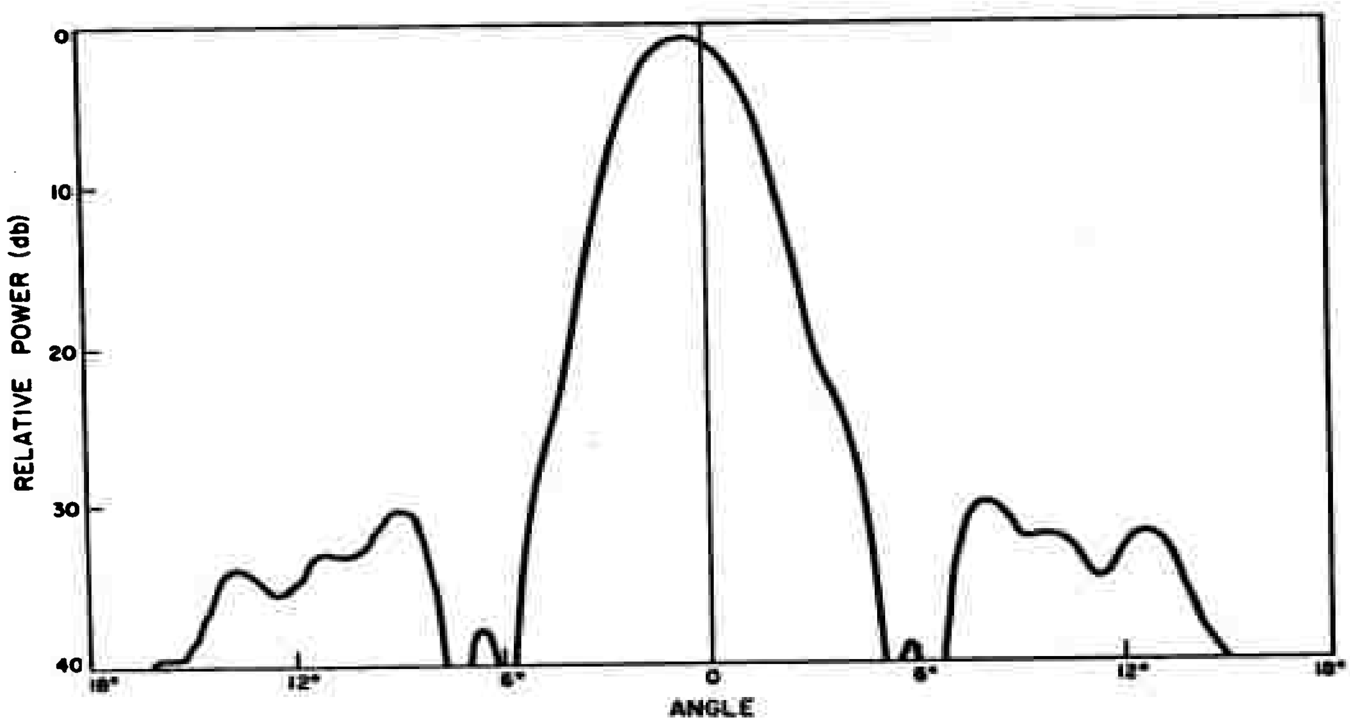

Figure 1.2 S-band antenna pattern, E-plane.

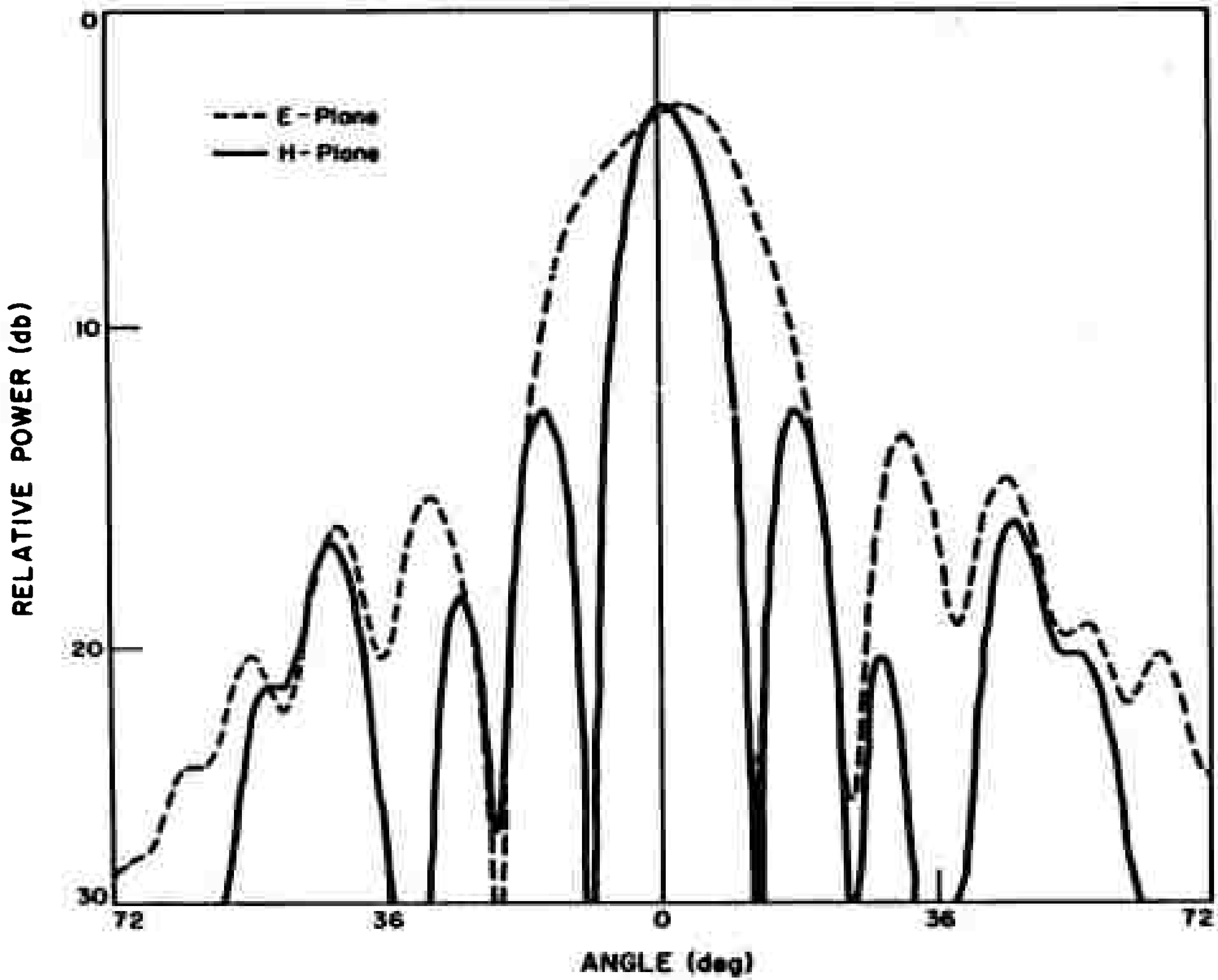

Figure 1.3 L-band antenna pattern, E- and H-planes.

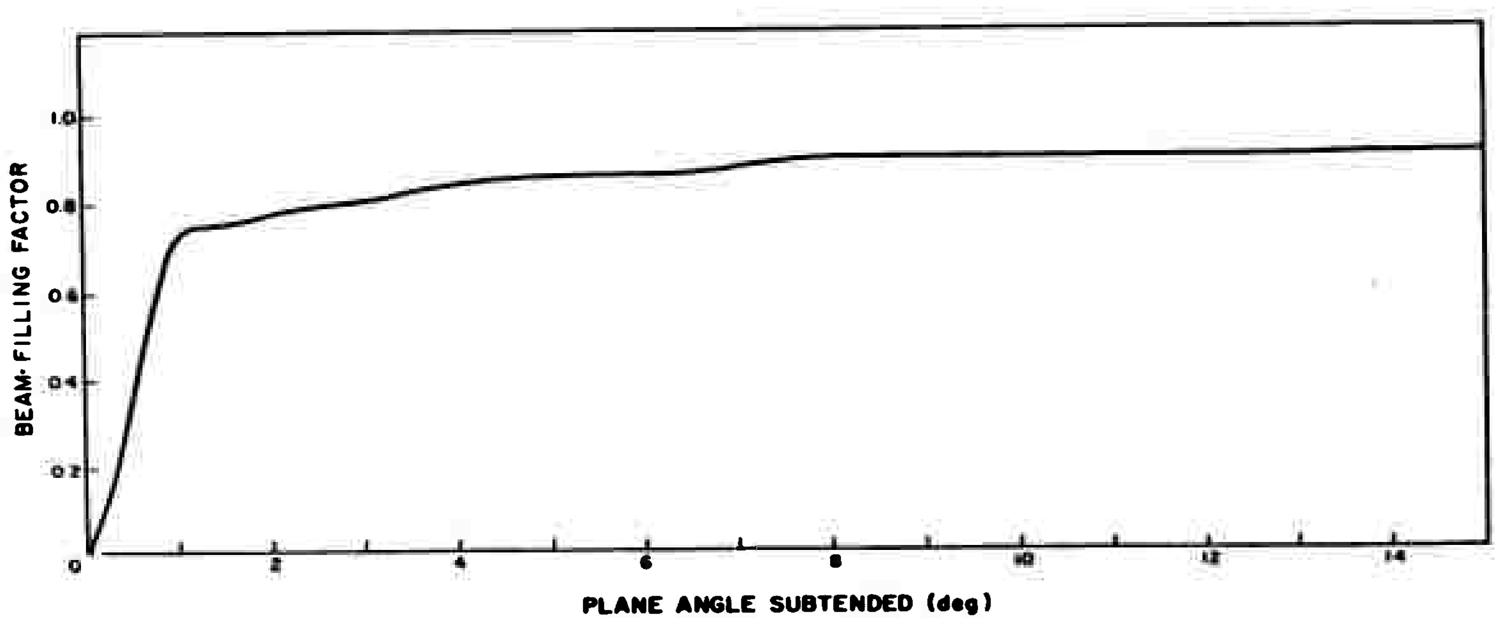

Figure 1.4 Beam-filling factor, K_a-band antenna.

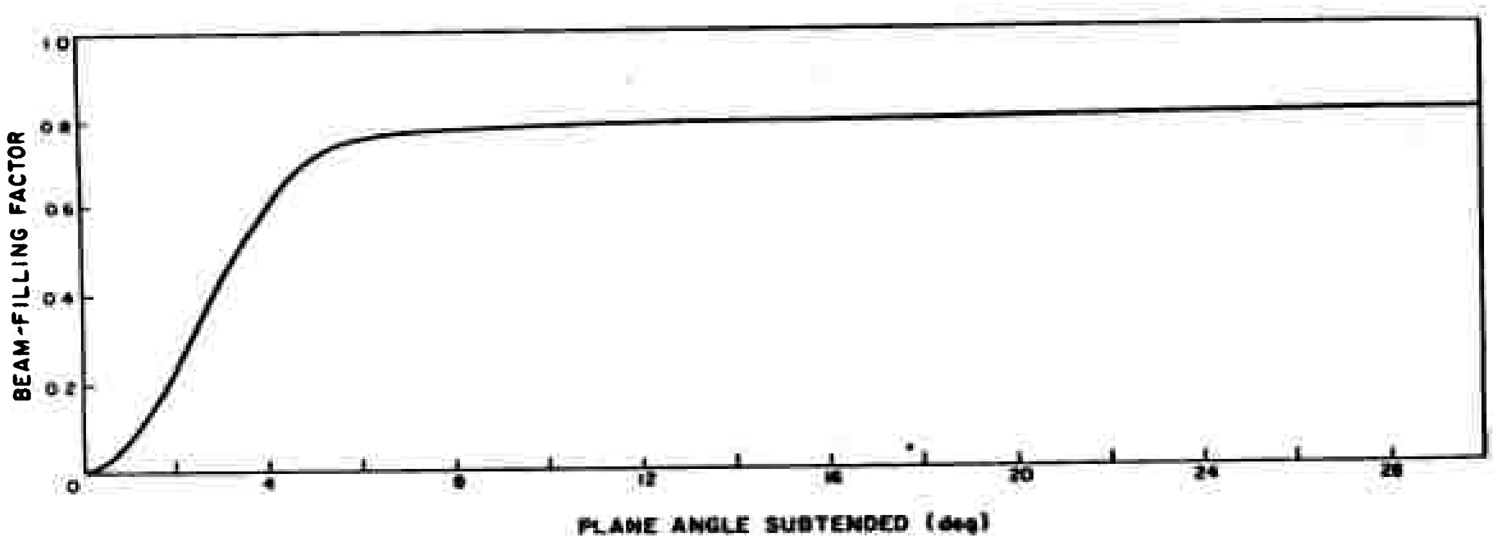

Figure 1.5 Beam-filling factor, S-band antenna.

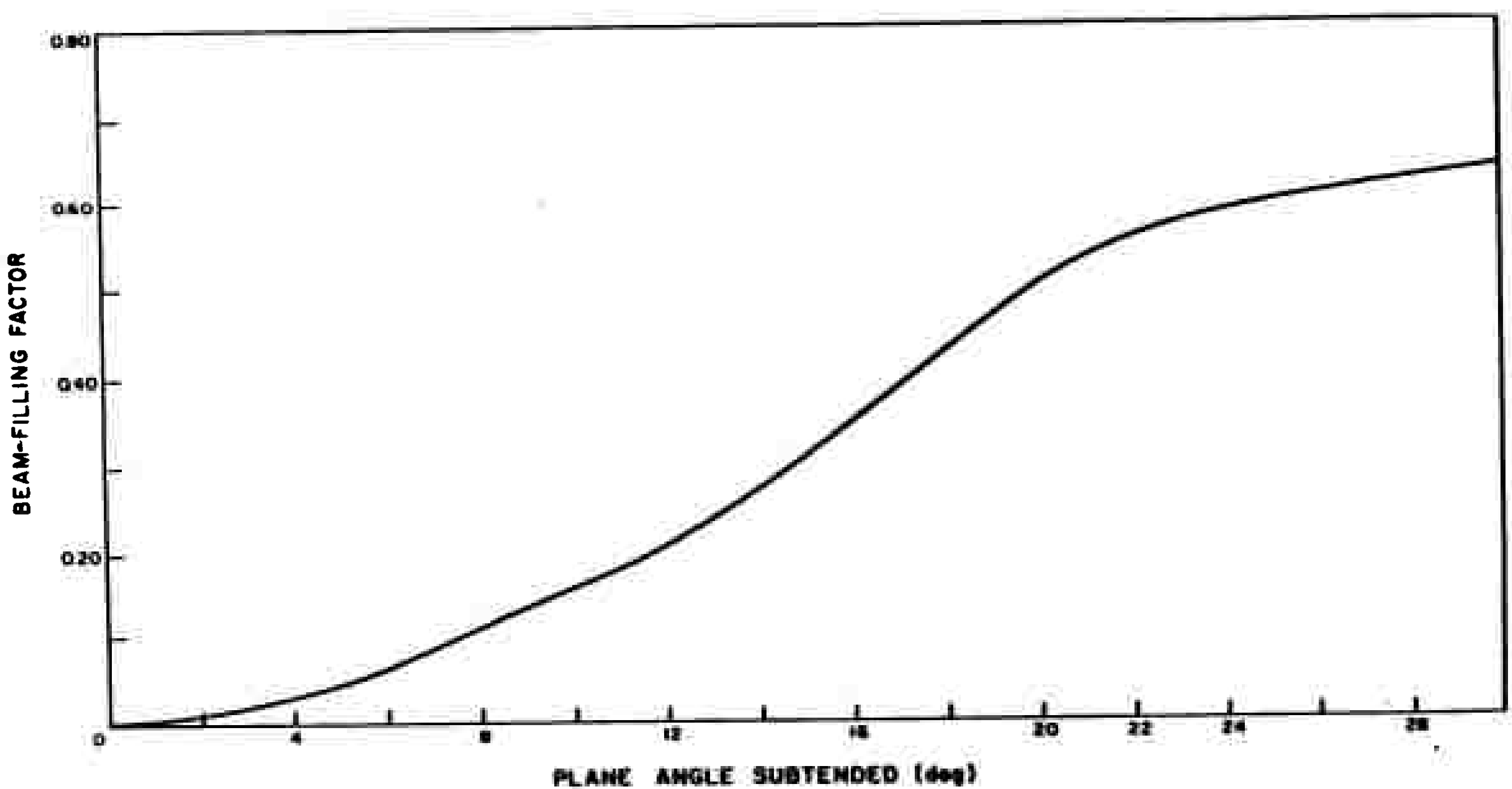

Figure 1.6 Beam-filling factor, L-band antenna.

CHAPTER 2

PROCEDURES AND INSTRUMENTATION

2.1 INSTRUMENTATION

The instrumentation utilized in the Lincoln Laboratory measurements on Johnston Island during the Fish Bowl Series included four complete radiometric systems operated at three widely separated microwave frequencies. Measurements of the electromagnetic characteristics of the nuclear bursts were made with these radiometers at K_a-band (34,450 Mc, vertical polarization), S-band (3000 Mc, vertical polarization), and at L-band (925 Mc, vertical and horizontal polarizations).

The K_a-band radiometer used a 4-foot parabolic antenna which provided a 0.6° beam at the half-power level with a maximum gain of 48.5 db. The gain pattern in the E-plane is shown in Fig. 1.1. The beam was nearly circularly symmetric, and the pattern in the H-plane is quite similar to the one shown. Referring to the block diagram of Fig. 2.1, the signal from the antenna passed through a ferrite switch which modulated the incoming signal at a 100-cps rate and compared it to that generated by a resistive termination whose temperature was known. A directional coupler between the antenna and the ferrite switch allowed the injection of known signal levels from an argon noise source which provided a convenient and reliable means of calibrating the difference in power between the antenna signal and the reference level. The signal out of the ferrite switch was converted to S-band by mixing it with the output of a 31,450-Mc klystron oscillator in a K_a- to S-band balanced mixer. This heterodyned signal was amplified in three series-connected low-noise, wide-band, travelling-wave amplifier tubes whose output was detected in a coaxial-type video detector. The passband of the K_a-band system was 900 Mc wide up to the detector which narrows it to a few megacycles and performs some integration.

The video signal at this point was recorded in a Precision Instrument tape recorder to a bandwidth of 100 kc. The video signal was also displayed on a Tektronix 545 oscilloscope where provision was made to photograph several minutes of the signal to a bandwidth of 50 kc with a Dumont Oscilloscope Camera, model 321A.

The first 50 microseconds of the video signal after burst time was displayed on a Tektronix 551 oscilloscope and photographed with a Fairchild camera, model 0-15A. This scope was triggered by the flash from the burst by means of a fiducial marker generator provided by Edgerton, Germeshausen and Grier, Inc. (EG&G). After the Star Fish shot, the L-band video was substituted for the K_a-band video in this set-up. The S-band video was displayed in this manner for all shots, but the photo-multiplier tube was damaged by the brilliance of the Blue Gill shot and failed to trigger for the last two shots.

The signal from the video detector was also amplified further by a narrow-band amplifier and fed into a synchronous detector which restored the dc level relative to the known reference signal. It was then integrated in two channels, one with a 0.1-second time constant and the other with a 1.0-second time constant and recorded on a Sanborn strip recorder. Two recording channels were provided for the 0.1-second data to provide a wide dynamic range for the signal whose magnitude was unknown prior to the measurement. The sensitivity of the 1.0-second integration time channel was such that a temperature variation of the order of $1^{\circ}K$ could be detected. Since the sensitivity is proportional to the square root of the integration time, the sensitivity of the faster recordings was correspondingly less.

The S-band system used an 8-foot dish whose beamwidth was 3° at half-power points as shown in Fig. 1.2, with a maximum gain of 33.8 db. The S-band dish was servo-slaved to the K_a-band dish, and their common pointing angle controlled by personnel in the van. A closed circuit television camera was boresighted on the K_a-band dish to monitor the field of view of the antenna and to aid in tracking the event.

The output of the S-band antenna after passing through a ferrite switch was amplified at S-band in a TWT amplifier. The rest of the S-band radiometer was identical to the K_a-band radiometer. The pass-band of the S-band radiometer was 2600 Mc to 3500 Mc for the Star Fish shot. Filters were added to narrow the acceptance band to 2750 Mc to 3450 Mc for the remaining events, in order to reduce the disturbance caused by radar interference. The sensitivity of the S-band system was better than 0.3°K temperature change in the 1.0-second integration channels for most of the measurements but was degraded to about 3.0°K by interference during the Star Fish event.

The L-band systems used a disk-loaded rod array as a stationary antenna. This array was arranged to provide two beams, one of which was horizontally polarized and the other vertically polarized. The gain profile of these beams, as seen in Fig. 1.3, had a 3-db width of 10° x 20°. The maximum gain of each beam was 20 db. Two complete radiometers, whose block diagram is shown in Fig. 2.2, were used at L-band to process the two polarizations separately. A solid-state switch was used to switch between the antenna and the reference level at a 1000-cps rate. Tunnel diodes were used as preamplifiers at L-band. These were followed by L-band to 30-Mc mixers and transistorized IF amplifiers. The video signals at the output of the IF amplifiers were recorded on the tape recorder and also were further amplified, synchronously detected, and integrated. The 0.1-second integration channels were recorded on Sanborn chart recorders and the 1.0-second integration channels fed into self-contained battery-operated Rustrack recorders.

The receiving bandwidth of the L-band radiometers was 4 Mc centered at 925 Mc. A 10°K antenna temperature change in the 0.1-second integration time channels could be reliably detected.

A Bolex 16-mm movie camera was mounted on the K_a-band antenna to monitor the field of view of the antennas. The antenna-pointing angles were recorded in analog form on a separate Sanborn recorder. Time, in the form of AMR, B-1 code, was recorded concurrently with the data in each recorder. The characteristics of all the instrumentation are summarized in Table 2.1.

The trailer and antennas are shown in Figure 2.3.

2.2 EXPERIMENTAL PROCEDURE

The experimental procedure followed in making measurements was quite similar for each nuclear test. Prior to burst time, the antennas were pointed at the predicted burst point with the single exception that, for Blue Gill, the L-band antenna was pointed 4° high to allow for the anticipated rise of that fireball.

At approximately H-30 minutes, all systems were calibrated by injecting known signal levels into the radiometers from their respective standard noise sources. The systems were calibrated again after the antenna temperature measurements for each event were completed. At the end of the series, the noise source calibrations were checked against a hot-cold load measurement. In this final calibration, the antennas were replaced by resistive terminations which were cooled to 0°C and then heated to 100°C. The calculated values of the noise sources in this region were confirmed by this measurement.

Measurements of the atmospheric attenuation at K_a-band were made about an hour before burst time. The total pre-shot transmission losses of the K_a-band and S-band systems were also checked by the method discussed in the previous section.

The tape recorders and the recording movie cameras were started at H-60 seconds. In the cases of the King Fish and Tight Rope events, the pointing angles of the S-band and K_a-band antennas were adjusted slightly a few seconds after burst to compensate for small errors in the burst point. After the initial signals had subsided, the antennas were scanned over the regions which seemed most appropriate to each case. In general, the duration of the signals was too short to permit a complete mapping procedure, but many of the significant features were determined before the signals vanished. Only in the case of Tight Rope was the image on the television monitor sufficiently distinct after the first few seconds to serve as a good visual aid to the scanning procedure.

TABLE 2.1 COMPARISON CHART OF INSTRUMENTATION

	K_a-band	S-band	L-band
Frequency	34,000-34,900 Mc	2750-3450 Mc (2,600-3,500 Mc, Star Fish only)	923-927 Mc
Antenna	Parabolic Dish 0.6^{o} beam Vert. Polarization	Parabolic Dish 3.0^{o} beam Vert. Polarization	Disk-Rod Array Hor. and Vert. Polarization
Sensitivity	$\Delta T = 1.0^{o}K$ (1 sec)	$\Delta T = 0.3^{o}K$ (1 sec) (Star Fish $3.0^{o}K$ (1 sec)	$\Delta T = 10^{o}$ K (0.1 sec)
Recording 1-sec Integration	Sanborn Chart Channel (1), 1^{o}-$500^{o}K$	Sanborn Chart Channel (4), 3^{o}-$500^{o}K$	Rustrack Chart Channel (1) (hor) 10-$500^{o}K$ Channel (2) (vert) 10-$500^{o}K$
0.1-sec Integration	Sanborn Chart Channel (2), 1^{o}-$500^{o}K$ Channel (3), 500^{o}-$5000^{o}K$	Sanborn Chart Channel (5), 1^{o}-$500^{o}K$ Channel (6), 500^{o}-$5000^{o}K$	Sanborn Chart Channel (7), 50-$5000^{o}K$ Channel (8), 50-$5000^{o}K$ (Large Outputs Compressed)
dc to 10,000 cps	P.I. Tape Recorder Channel (1), FM	P.I. Tape Recorder Channel (3), FM	P.I. Tape Recorder Channel (5), FM
100 to 100,000 cps	P.I. Tape Recorder Channel (2), direct	P.I. Tape Recorder Channel (4), direct	P.I. Tape Recorder Channel (6), direct
dc to 50,000 cps	Dumont Camera 545 Scope	Dumont Camera 545 Scope	--------
10 kc to 10 Mc	Fairchild Camera 551 Scope Fiducial Trigger (Star Fish only)	Fairchild Camera 551 Scope Fiducial Trigger	Same as S-band (except Star Fish)
Antenna Position	Sanborn Chart Channels 9 and 10 Kintel TV Monitor Bolex Camera	Same as K_a-band	Fixed
Timing Marks	All Recorders	All Recorders	All except Rustrack

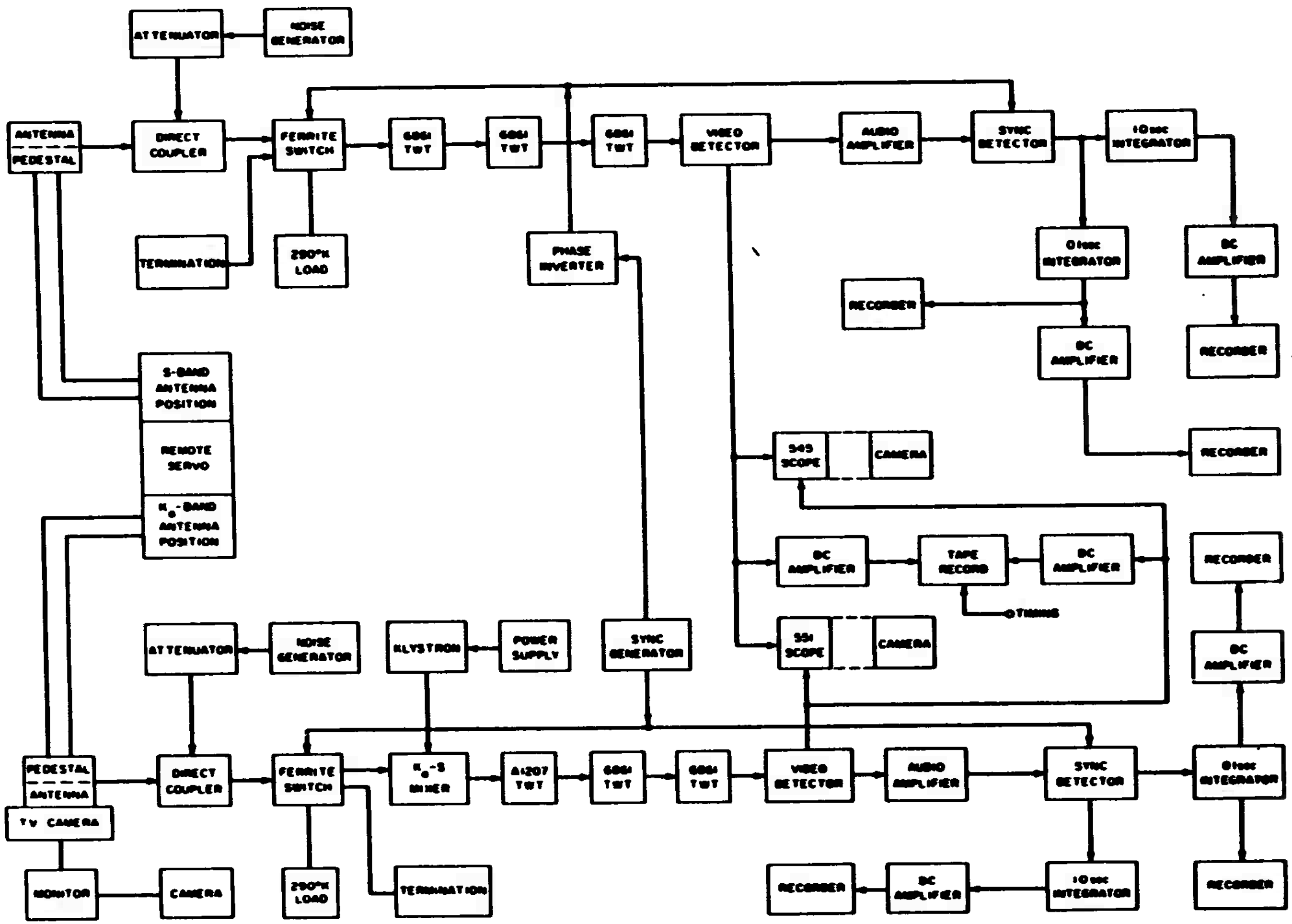

Figure 2.1 Block diagram of K_a - and S-band radiometers.

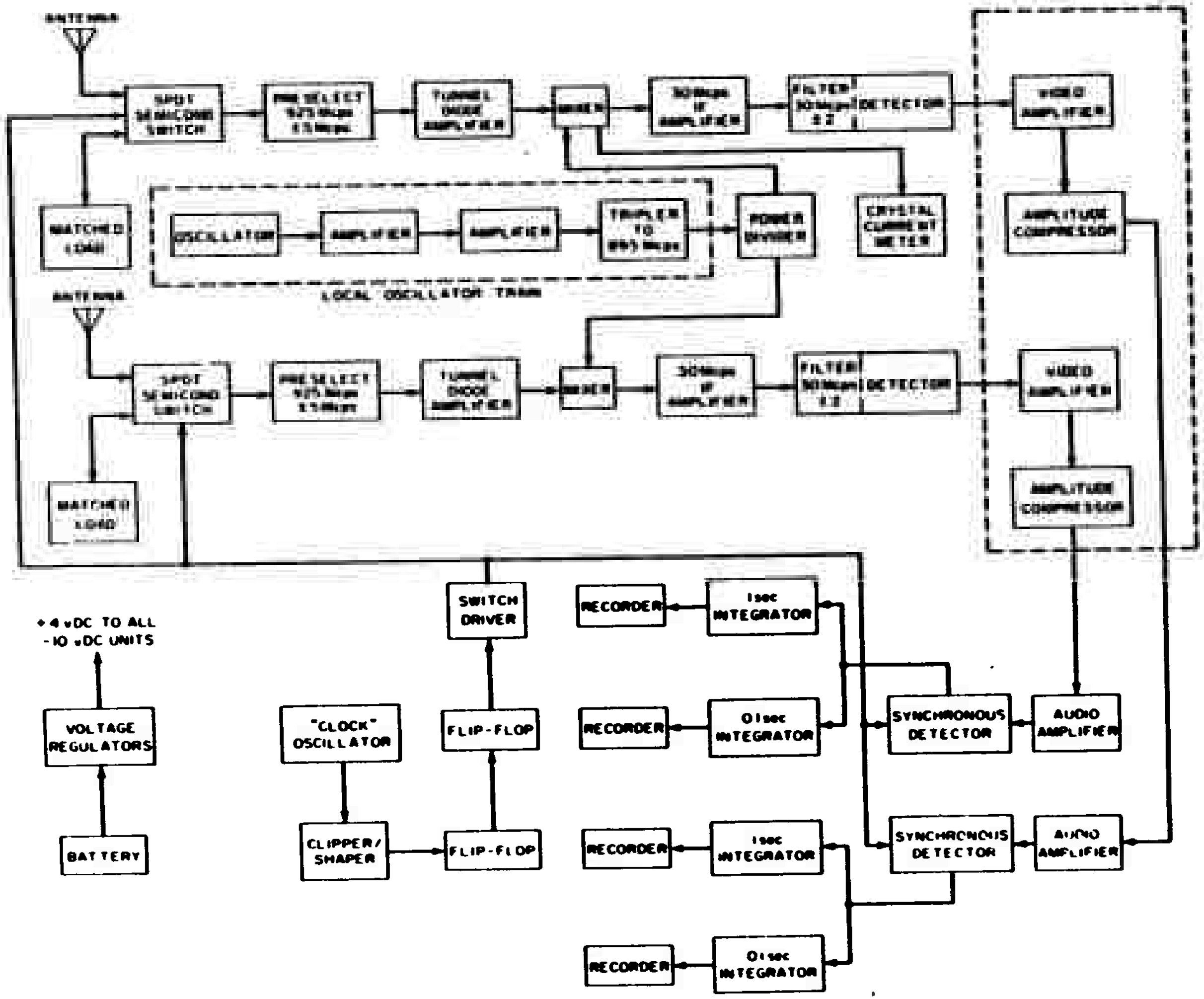

Figure 2.2 Block diagram of L-band radiometer.

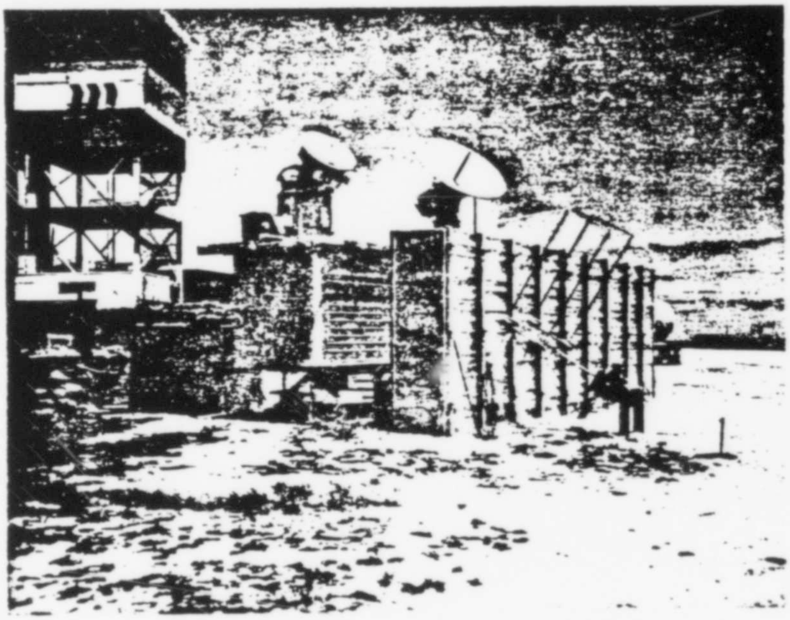

Figure 2.3 View of trailer and antennas. (DASA 26-6663-62)

CHAPTER 3

RESULTS

The results in the interim report have been re-examined in detail and supplemented with additional data from the faster channels. The corrections which have been made were minor, occurring principally during the beginning of the signals where the 0.1-second integration channels were sometimes too slow to follow the rapid changes closely. Where appropriate, the early time response has been plotted on an expanded scale from the wide bandwidth data. The precision of the data from the faster channels is, of course, lower than that which is derived from channels with longer integration times.

Initial examination of the L-band results indicated somewhat higher (10-20%) temperatures for the horizontally polarized output. Subsequent study of data taken of the sun at the field installation with this system shows the same difference, which must be therefore ascribed to a difference in efficiency in the two sections of the L-band antenna. It was consequently concluded that there was no appreciable difference in the data recorded for the two polarizations at L-band for any of the nuclear shots. The results presented here apply equally well to either polarization.

The K_a-band results presented here have been corrected for the average atmospheric loss measured prior to each shot.

The antenna position angles for the K_a-band and S-band antennas are plotted simultaneously with the antenna temperature data as a function of time in order to allow interpretation of the effects of scanning the antennas directly from the data.

3.1 STAR FISH PRIME

The Star Fish burst occurred very close to the planned location, thus presenting negligible error in the initial pointing angles of the antenna. The radiation and debris from the Star Fish shot expanded essentially unimpeded as a consequence of the high altitude (400 km) of the burst. Unlike the lower shots, its boundaries were indistinct and its geometric extension difficult to specify. It is evident, however, that it spread over a region much larger than that encompassed by the radiometric antenna beams in a very small fraction of a second.

3.1.1 K_a-band. In marked contrast to the results of the lower shots, the antenna temperature change of the K_a-band system was less than the minimum detectable signal of 1^{o}K. As will be seen in later discussion, this result is a consequence of the fact that the Star Fish radiation did not increase the electron-ion density sufficiently in either the burst region or in the intervening atmosphere to change the absorption of K_a-band radiation significantly.

3.1.2 S-band. At burst time the S-band antenna temperature shown in Fig. 3.1 rose immediately by 42^{o}K. (Note: The Star Fish results were previously given in terms of the temperature change at the radiometer and, therefore, smaller by the amount of the transmission line loss.) The initial peak decayed after a few seconds to a minimum of 7^{o}K at 15 seconds and then climbed slowly to a broad secondary peak of 20^{o}K in the next 30 seconds. This effect vanished after three or four minutes.

3.1.3 L-band. The L-band antenna temperature shown in Fig. 3.2 rose immediately by 300^{o}K at burst time, dipped to 80^{o}K at 15 seconds, and then rose slowly to 112^{o}K at 40 seconds. It, likewise, vanished in three to four minutes.

3.2 CHECK MATE

The Check Mate burst was about 2° below and 2° east of the expected direction. The burst spread rapidly and filled the S- and K_a-band antenna beams in a small fraction of a second. Table 3.1 gives representative values of the angle subtended by the diameter of the Check Mate fireball at the radiometric antennas as taken by the Bolex boresighted camera and from Reference 4. The burst was quite

symmetrical, but the edges were irregular and indistinct, causing an uncertainty of ± 15% in the listed values.

The peak antenna temperatures recorded for the Check Mate shot were considerably greater than anticipated and proved to be the highest encountered during the series at each frequency.

3.2.1 K_a-band. The K_a-band antenna temperature, as shown in Figs. 3.3 and 3.4, rose to a peak value

It remained at the peak value for only a fraction of a second before decaying rapidly in a nearly exponential manner, reaching half value in less than 2 seconds and vanishing in about 60 seconds.

3.2.2 S-band. The S-band antenna temperature (Figs. 3.5 and 3.6) rose to a peak temperature

The decline was slower than K_a-band, half value occurring in about 6 seconds. At 40 seconds the temperature stabilized at about

Scanning the antenna upward by 10° to the new center of the burst showed a slightly higher temperature in that region. Scanning the antenna downward 60 seconds after the burst indicated a distinct bottom boundary of the microwave source 3° below the burst point, although the antenna beam was still overlapping the edge of the fireball. At 110 seconds the antenna was scanned in azimuth across the nuclear cloud, and the width of the microwave source at the burst point elevation was found to be about 18°. (Note: The angular motion of the antenna is equal to the azimuth change multiplied by the cosine of the elevation angle.) By 120 seconds the cloud was about 10% cooler in the center, with the maximum temperature occurring halfway from the center to the edge.

<u>3.2.3 L-band.</u> The L-band antenna temperature (Figs. 3.7 and 3.8) rose more slowly than for the other two frequencies, reaching a peak

It

decayed somewhat more slowly than the S-band.

3.3 KING FISH

The King Fish burst occurred 0.2° above and 1.2° west of the direction of the pre-pointed antennas. The peak antenna temperatures were lower than those for Check Mate but similar in character and duration.

The burst expanded asymmetrically upward. The angular dimensions in Table 3.2 were derived from E G & G photography on Johnston Island and from the Bolex Camera mounted on the K_a-band antenna.

<u>3.3.1 K_a-band.</u> The K_a-band antenna temperature (Figs. 3.9 and 3.10) rose in less than 10 milliseconds. A small correction in the pointing angle at seven to nine seconds had no obvious effect on the antenna temperature. The rather abrupt changes in slope at 2 to 5 seconds were not associated with antenna motion but were probably the result of early time fluctuations in the fireball (Reference 5). At 15 seconds the bottom edge of the microwave source was located 2° below the initial pointing angle. The antenna was scanned upward starting at 18 seconds, encountering somewhat higher temperature. The whole area became transparent to K_a-band after 25 to 30 seconds.

3.3.2 S-band. The S-band antenna temperature (Figs. 3.11 and 3.12) required about 1 second to reach a peak

At 60 seconds the upper edge of the S-band radiation source was 30° above the burst point as a consequence of the fast rise and asymmetrical expansion of the debris. Scanning the antenna in azimuth at 150 seconds indicated that the central region was then 20° in diameter with a source temperature of about 100°K. At 250 seconds a northern portion of the sky was scanned briefly in an attempt to detect the beta patch, but no region of excess temperature was located.

3.3.3 L-band. The L-band excess antenna temperature for King Fish, shown in Fig. 3.13, rose 650°K in 2 seconds and fell at very nearly the same rate as at S-band. The smaller antenna temperatures at L-band observed for the lower shots with their smaller fireballs are due primarily to the smaller fractional filling of the antenna beam.

3.4 BLUE GILL TRIPLE PRIME

The Blue Gill burst was 1.6° below and 1° west of the expected direction. The Blue Gill fireball proved to be quite difficult to scan systematically, since it rose rapidly in elevation and its image on the closed-circuit television monitor was not well defined after the first few seconds. Therefore, the antenna elevation was raised periodically to compensate for the anticipated rise. Supplemental data taken by the Bolex movie camera boresighted on the antenna to record the scanning aspect was unfortunately lost during laboratory processing.

The angular dimensions in Table 3.3 were furnished by EG&G.

3.4.1 K_a-band. The K_a-band antenna temperature (Figs. 3.14 and 3.15) rose 750°K at burst time and held this value for 2 seconds before climbing to a peak The temperature remained near its peak value for over 30 seconds before dropping sharply and disappearing after 60 seconds.

3.4.2 S-band. The S-band excess antenna temperature (Figs. 3.16 and 3.17) after a short initial impulse at burst time held a value of 240°K for 4 seconds and then climbed slowly to a peak After a few seconds at the peak value, it decayed somewhat more slowly than it rose. At 100 seconds the antenna was scanned across the area, and the edge of the torus, which was well formed at that time, was found to be considerably hotter than the central region.

The photographic record was indistinct earlier than 30 microseconds, and quantitative data cannot be presented for that region. The technique used for recording the very early time response (Chapter 2) was somewhat of an incidental appendage to the radiometry system and was not nearly as useful in obtaining data as the techniques for later times proved to be. In addition to the anticipated handicap caused by the periodic switching of the antenna signals by the radiometers, the fiducial marker failed to trigger the oscilloscope for several of the events. In any future measurements of this type, it is recommended that special receivers, separate from the radiometers, be developed to investigate the first few microseconds of the response.

The electromagnetic impulse (Fig. 3.18) was calibrated in terms of antenna power

Data from the tape recorder indicate that very similar impulses occurred for the other shots, at least in those cases where the impulses were not obscured by an immediate rise in the thermal signal.

3.4.3 L-band. The L-band antenna temperature (Fig. 3.19) rose to 240°K shortly after burst. It held this value for several seconds but then declined slowly to 190°K at 25 seconds before climbing to a new peak of 350°K at 65 seconds. As previously indicated, the L-band antenna was pre-pointed above the burst point, and the large secondary peak appears to be the result of the rise of the fireball through the center of the beam.

3.5 TIGHT ROPE

The Tight Rope burst was 3/4° above and 1/4° east of the predicted direction. Angular dimensions of the visible fireball are given in Table 3.4.

3.5.1 K_a-band. The K_a-band antenna temperature (Figs. 3.20 and 3.21) increased 300°K

As in Blue Gill, it held this initial value for about a second before climbing

The sharp drop at 12 to 13 seconds occurred shortly before the hole in the torus became visible.

3.5.2 S-band. The S-band signal (Figs. 3.22 and 3.23) exhibited an impulse response at burst similar to Blue Gill and settled to 240°K in a fraction of a millisecond. It held this value 2.5 seconds and climbed to a peak At 58 seconds the top edge of the radiating region was 7° above the initial point, and at 68 seconds the bottom edge was 2° below the initial pointing angle. The effect of the cooler hole in the torus was evident during this scan, but its size was considerably smaller than the main lobe of the S-band antenna. The signal decayed at about the same rate as the higher shots.

3.5.3 L-band. The L-band antenna temperature rose 55°K at burst time (Fig. 3.24). The much smaller temperature change is consistent with the smaller fireball size relative to the broad L-band antenna beam. The small signal combined with an uncertainty in measurement of $\pm 10^{\circ}$K admits a fairly sizeable percentage error in this case. The inaccuracy in the antenna temperature data in the other cases is less than 10% for the major portion of the measurement interval.

TABLE 3.1 ANGULAR SIZE OF FIREBALL, CHECK MATE

Time sec
0.1
1.0
10.0
30.0 - 100.0

TABLE 3.2 ANGULAR SIZE OF FIREBALL, KING FISH

Time sec	Horizontal Diameter degrees	Vertical Diameter degrees
0.1		
0.5		
1.0		
6.0		
10.0		
20.0		
40.0		
60.0		

TABLE 3.3 ANGULAR SIZE OF FIREBALL, BLUE GILL

Time	Outside Diameter		Torus Opening	
sec	Horizontal degrees	Vertical degrees	Horizontal degrees	Vertical degrees
0.15				
0.5				
1.0				
2.0				
9.0				
15.0				
27.0				
45.0				
69.0				
81.0				
99.0				
102.0				

TABLE 3.4 ANGULAR SIZE OF FIREBALL, TIGHT ROPE

Time sec	Outside Diameter Horizontal degrees	Outside Diameter Vertical degrees	Torus Opening Vertical degrees
0.1			
0.4			
1.0			
3.0			
5.0			
10.0			
20.0			
30.0			
35.0			
50.0			
90.0			

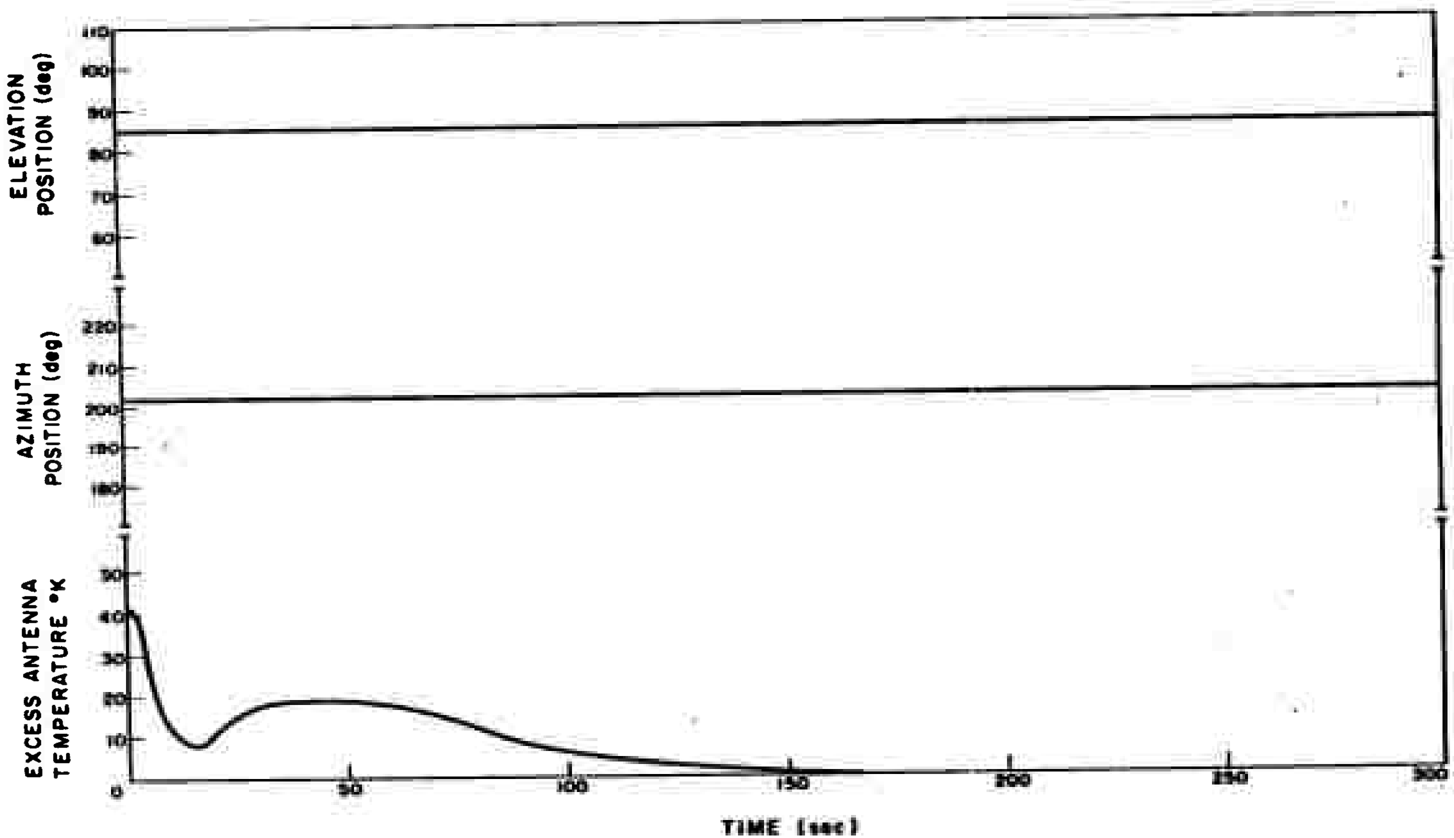

Figure 3.1 Excess antenna temperature, S-band, Star Fish.

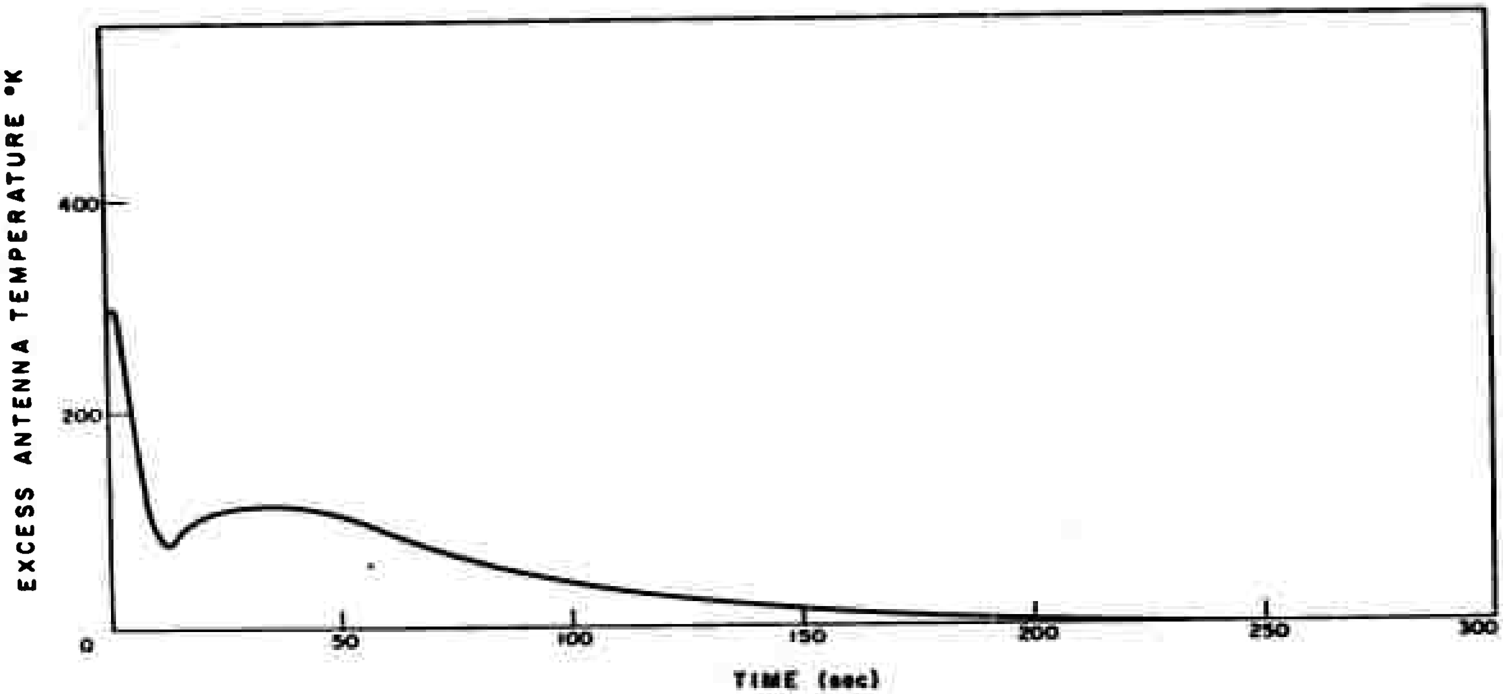

Figure 3.2 Excess antenna temperature, L-band, Star Fish.

Pages 48 - 57 deleted.

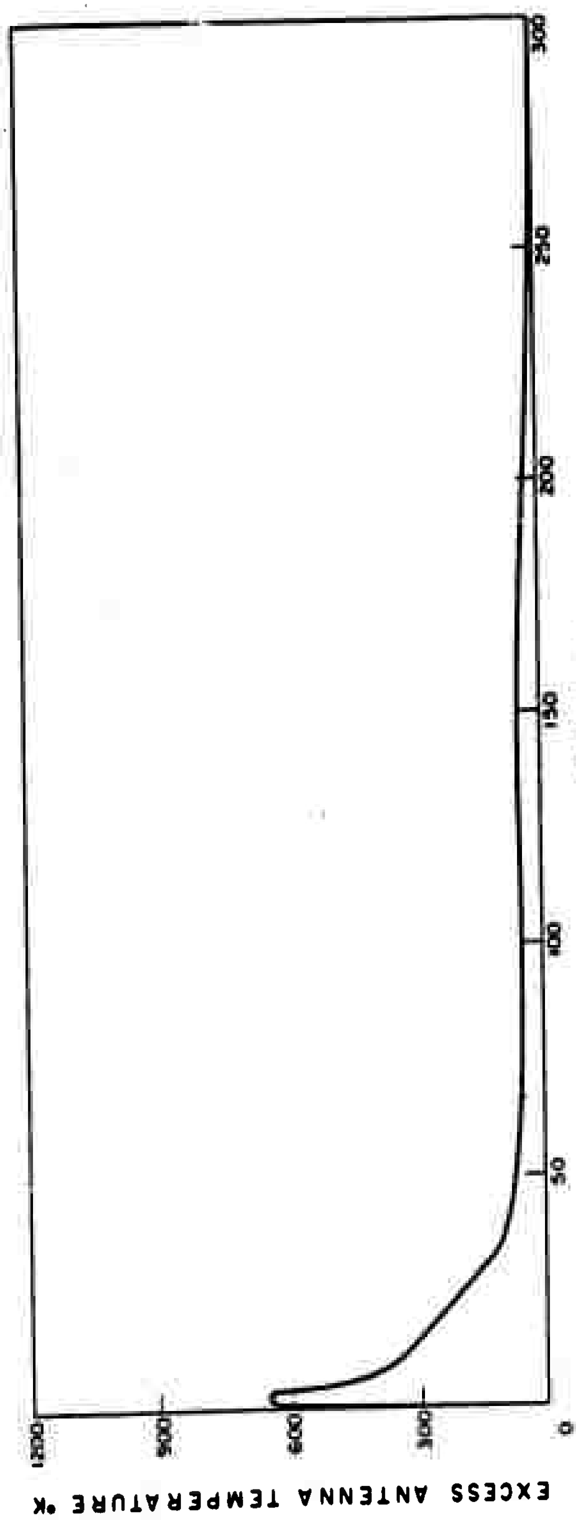

Figure 3.13 Excess antenna temperature, L-band, King Fish.

Pages 59 - 61 deleted.

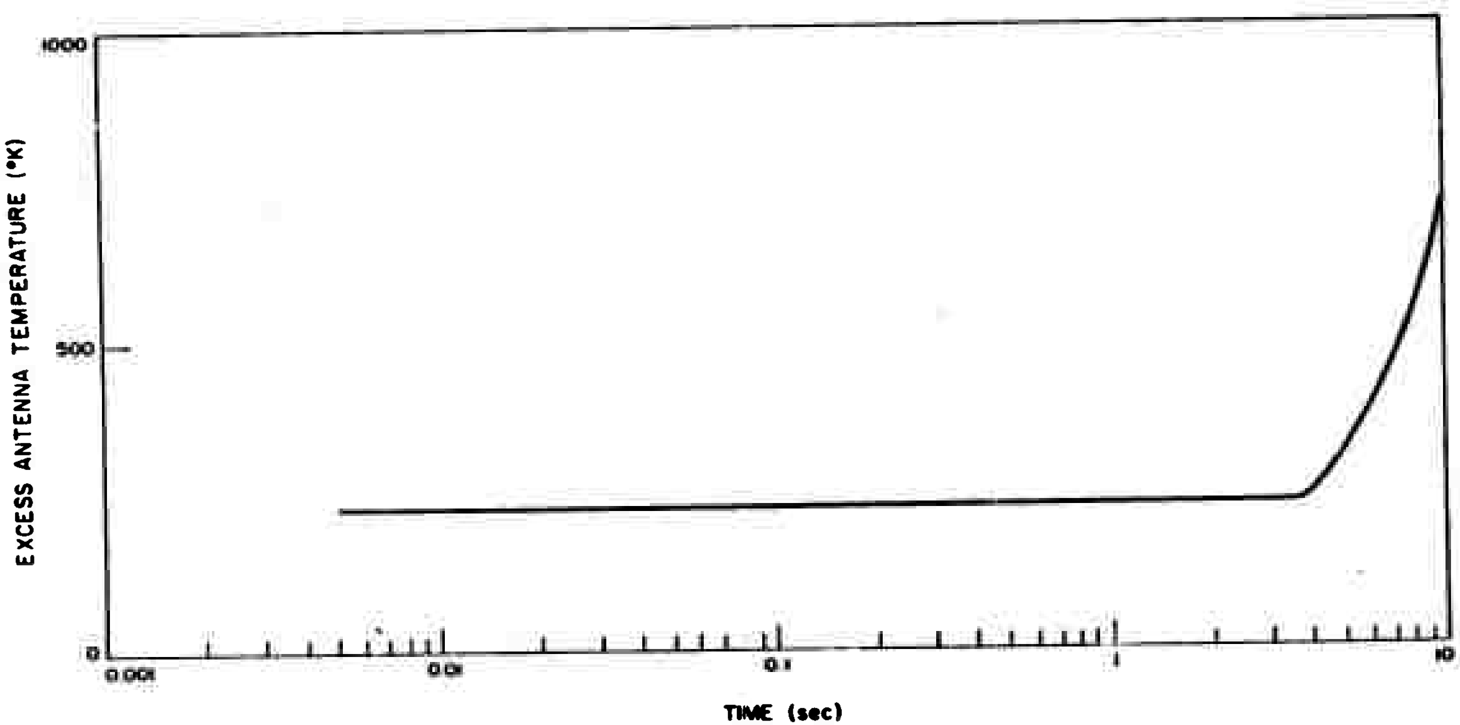

Figure 3.17 Excess antenna temperature, expanded scale, S-band, Blue Gill.

Page 63 deleted.

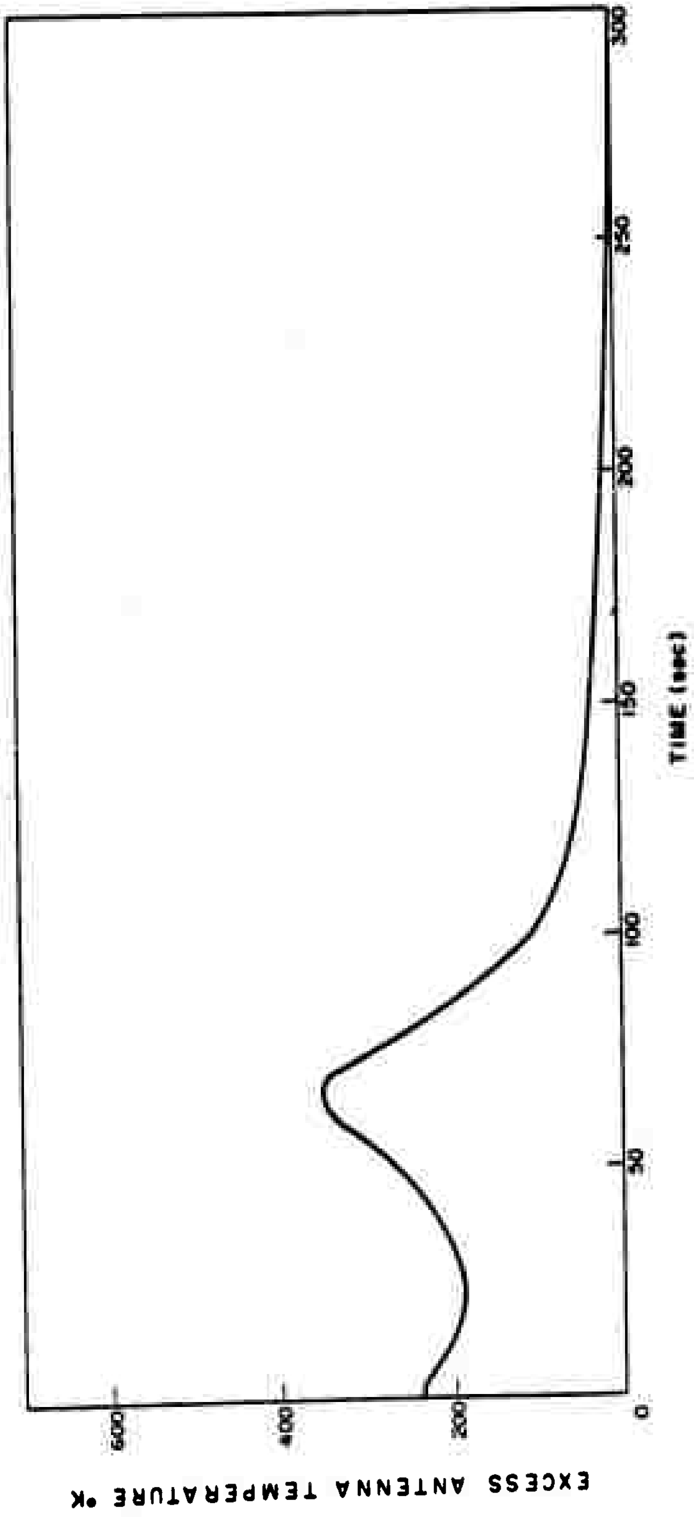

Figure 3.19 Excess antenna temperature, L-band, Blue Gill.

Pages 65 - 67 deleted.

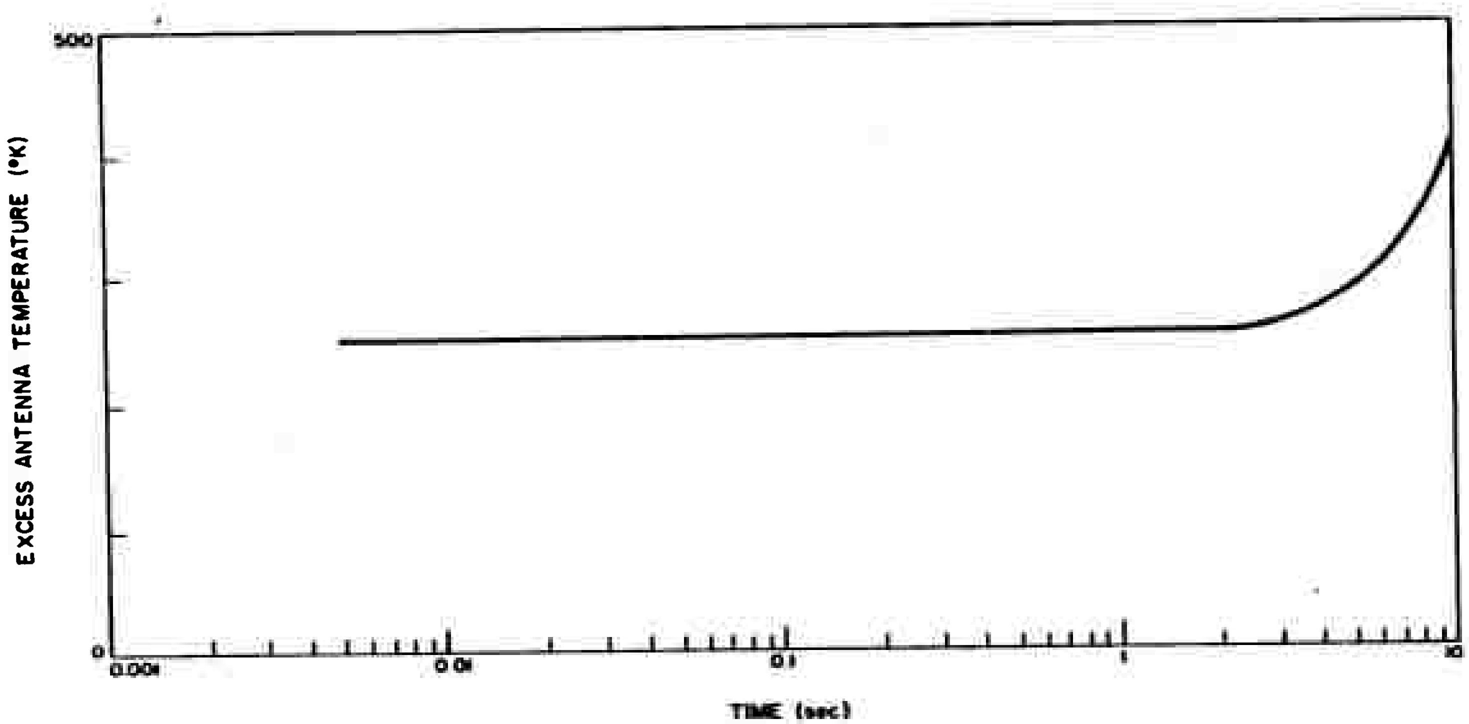

Figure 3.23 Excess antenna temperature, expanded scale, S-band, Tight Rope.

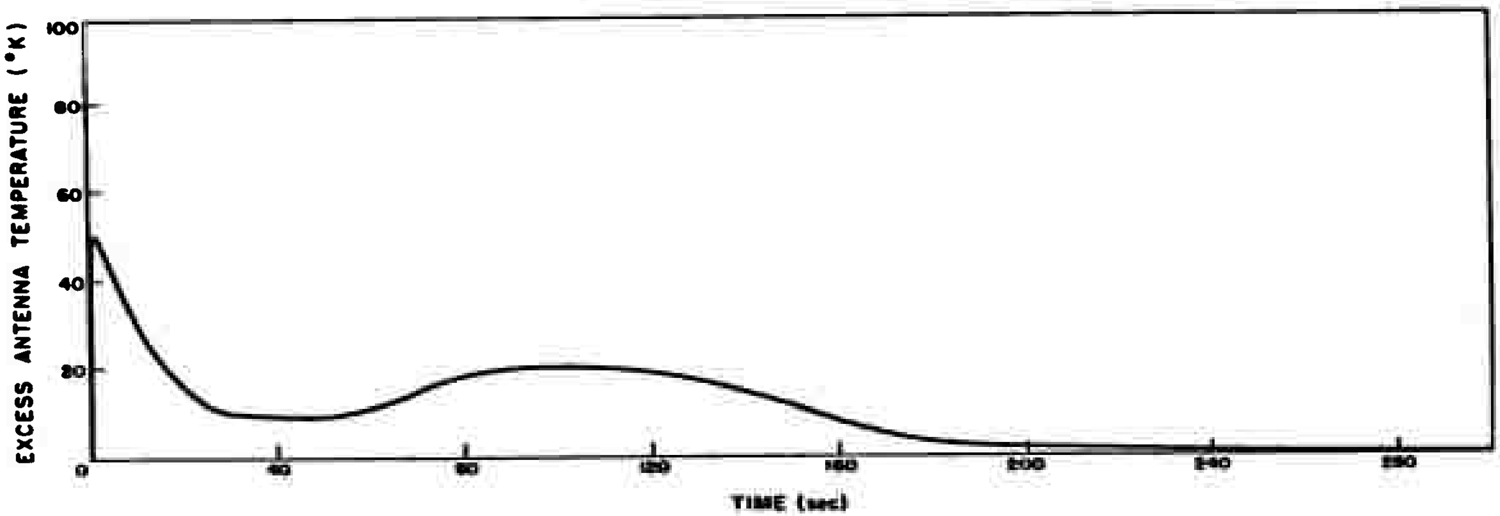

Figure 3.24 Excess antenna temperature, L-band, Tight Rope.

CHAPTER 4

DISCUSSION

An important factor in the interpretation of the data is the integration effect of the antenna beam size, at least in instances in which the main lobe encompasses an area greater than that which is being investigated. As previously indicated (Section 1.2), it is not possible to obtain a complete solution for all the conditions encountered in practice. In order to provide a basis for interpreting the antenna effect, the following procedure was adopted. The emission temperatures (i.e., $(1 - \tau)\ T_B$) for spherically shaped radiators which would yield the observed antenna temperatures during the time intervals of interest were calculated. The radii of the hypothetical radiators were taken to be equal to the average radius of the visual fireball (see Tables 3.1 through 3.4), and the centers of these spheres were located in the direction of maximum gain of the antennas (Figs. 1.1, 1.2, and 1.3). No attempt was made to account for the nonuniformity of the temperature within the fireball proper except that data points were selected for the direction of maximum antenna temperature. There is some experimental justification for this approach in the fact that, with the exception of the well-developed hole in the torus for Blue Gill and Tight Rope, the antenna temperature was not a sensitive function of direction within the fireball area. The results of these calculations are shown in Figs. 4.1, 4.2, 4.3, and 4.4 for Check Mate, King Fish, Blue Gill, and Tight Rope, respectively.

4.1 CHECK MATE

Referring to Fig. 4.1, depicting the calculated equivalent emission temperature $T_B(1-\tau)$ for the Check Mate shot, several observations may be made.

The decay of the exceptionally high initial temperatures is very nearly exponential over the time interval considered. The K_a-band temperature dropped rapidly after one-half second, while the S-band temperature remained relatively constant for two seconds before starting the exponential decay. (The possibility of calculating the equivalent temperatures at very early times is precluded by the initial error in the burst position.) Consideration of this result in conjunction with the fact that the K_a-band temperature was consistently higher than the emission temperatures at the other two frequencies for the lower altitude shots during this time interval, but very much lower for the Star Fish shot, leads to the conclusion that the Check Mate burst was becoming transparent to K_a-band radiation in less than one second.

At one and a half seconds the K_a-band temperature is one-half the S-band temperature, the latter of which is presumably a good measure of the debris temperature at this time. Therefore, the transmission coefficient for K_a-band at one and a half seconds is equal to one-half ($\tau_B \approx 1/2$), which is equivalent to an attenuation of 3 db. Rough estimates of the average electron density may be obtained by applying this result to the expression for the attenuation in a fully ionized plasma (Eq. 1.8). A uniform layer of thickness equal to the diameter of the burst is assumed. The results are $n(e) \approx 6 \times 10^{10}$ cm^{-3} at one and a half seconds. Likewise, the results shown in Figs. 3.5 and 3.7 indicate that the transmission coefficient of the debris at S-band reaches the value of one-half at about 165 seconds, so that the electron density is then found to be $n(e) \approx 10^9$. This latter value leads to an estimate of the effective recombination coefficient, $\alpha = \frac{1}{nt} \sim 6 \times 10^{-12}$. The value of n(e) at 1.5 seconds is consistent with this value of α if the original value of the electron density $n_o(e) \sim 2 \times 10^{11}$ cm^{-3}.

The attenuation through the fireball region may be obtained for other frequencies from these values since, as shown in Eq. 1.8, the attenuation varies as the inverse square of the frequency. For example, the attenuation at 300 Mc at t = 165 seconds would be 300 db, indicating a formidable UHF-radar barrier for a period of minutes after the burst.

The fact that the L-band temperature is consistently lower than the S-band temperature may be an indication that the L-band absorption occurs in a cooler layer than at S-band. The uncertainty entailed in the antenna beam correction for L-band is nearly as large as this temperature difference, however. The rise in the L-band antenna temperature after three seconds is explained by the visual fireball spreading into the antenna beam, but the distinctive dip at three seconds is a separate unexplained effect which may be associated with a rapidly dissipated absorption layer outside the fireball proper.

4.2 KING FISH

The equivalent emission temperatures calculated from the King Fish antenna temperatures are shown in Fig. 4.2. The initial temperatures decayed as an exponential function of time. The emission temperature at K_a-band was higher than at the lower frequencies for the first five seconds. This behavior in conjunction with the results for the other shots may be interpreted as concrete evidence that the K_a-band radiation originates in a deeper (i.e., hotter) layer of the fireball. The other possible explanation, that the temperature was higher in the localized surface area probed by the K_a-band antenna, seems to be refuted by the small effect of scanning the beam within the fireball.

At about 12 seconds the K_a-band emission temperature falls to half that of S-band, indicating 3 db of attenuation through the fireball at K_a-band.

fireball diameter of 70 km and a temperature of 2100°K, leads to an

The

recombination coefficient estimated from this result is $\alpha \approx \frac{1}{nt} \approx 8 \times 10^{-12}$/sec.

4.3 BLUE GILL TRIPLE PRIME

The emission temperatures calculated from the Blue Gill antenna temperatures are shown in Fig. 4.3.

tained its initial temperature for a much longer interval than the higher

The K_a-band temperature is considerably higher than for the lower frequencies during this interval. This large difference emphasizes a shortcoming in the geometrical model of the fireball assumed for the emission temperature calculations.

Without quantitative data on the extent of this region, it is not possible to calculate emission temperatures until after the effect of the ionized sheath has dissipated. An estimate of the one-way attenuation of the sheath along a radial path between the fireball and the antenna at one second for K_a-band may be made by extrapolating the emission temperature in Fig. 4.3 to this time and applying the results with the antenna temperature data from Fig. 3.15 to the relation

$$T_A = \tau_M T_B F_B = (1 - \tau_M) T_M$$

from which the transmission coefficient $\tau_M \approx 0.094$, and the attenuation $L_A = \frac{1}{\tau_M} \approx 10.6 = 10.3$ db.

4.4 TIGHT ROPE

The Tight Rope fireball maintained its initial peak temperature for a shorter period (Fig. 4.4) than Blue Gill.

As in the case of Blue Gill, an attenuating sheath of ionized atmospheric material formed around the fireball within a few microseconds after the burst.

The transmission coefficient of the sheath for K_a-band along a radial path could be calculated from the antenna temperature of 330°K and the beam-filling factor of 0.8 at one-half second if the emission temperature were known.

The inverse square of the frequency dependence for attenuation translates this result into 130 db at S-band.

Scanning the antenna to the edge of the fireball at 60 seconds (see Fig. 3.22) indicates quite decisively that the attenuation at S-band had become negligible outside the visual fireball by that time, while the fireball itself was still opaque to S-band signals. Furthermore, the sudden rise in the antenna temperature at 0.7 second at K_a-band, at 8 seconds at S-band, and at 25 to 35 seconds at L-band strongly suggest that the attenuation of the sheath was becoming negligible for these frequencies at these respective times.

4.5 STAR FISH PRIME

The microwave effects of the Star Fish shot were strikingly less than for the lower shots. The debris region was quite transparent to radiation at frequencies at least as low as S-band. It is not yet completely clear whether that attenuation which was observed occurred primarily in the debris region or in the atmosphere ionized by the burst. Since the L-band temperature rose somewhat higher than the upper atmospheric temperature, it appears likely that at least part of the attenuation occurred in the debris region. The emission temperature of the debris cannot be deduced from the radiometric data alone, since the region was nearly transparent to the radiometric frequencies. If the attenuation is assumed to occur in a region with an emission temperature of the order of 10,000°K, then from the L-band data at one second $L_B \approx 1.03 = 0.15$ db for L-band radiation and from the S-band data $L_B \approx 1.004 = 0.017$ db for S-band signals. On the other hand, if the absorption occurred in the ionized atmosphere with an assumed temperature $\approx 300°$, the S-band data yields $L_M \approx 1.15 = 0.6$ db for S-band radiation at one second after burst.

Pages 76 - 79 deleted.

CHAPTER 5

CONCLUSIONS AND RECOMMENDATIONS

The microwave radiometric measurements have provided quantitative data on the amount of thermal noise incident on radar-type antennas as a result of high-altitude nuclear bursts. These results are given explicitly by the radiometric data without need for elaborate calculation or interpretation. For example, a radar receiver with an antenna beamwidth of a few degrees or less must anticipate thermal noise input

The microwave noise for intermediate altitudes scales very nearly linearly with the altitude. At 400 km there is much less noise generated by the burst since the debris is transparent to frequencies above S-band. The peak noise temperatures appear to be nearly independent of the yield of the weapon. The sensitivity of low-noise radar receivers will be sharply reduced by this noise. For example, a receiver with a noise figure of 3 db will become approximately 10 db less sensitive for a few seconds if its antenna is pointing toward a burst, and false targets may be indicated by target threshold circuits.

The attenuation results deduced from the radiometric data are valuable supplements to attenuation data obtained by other means. Illustrative examples of the deductions are given in the previous chapter. A reliable determination of the attenuation may be made from the radiometry data directly in those cases in which the medium is partially transparent to one of the radiometer frequencies at the same time that it is nearly opaque to another (lower) frequency from which the temperature of the medium may be determined.

The attenuation of the Star Fish shot was negligible for K_a-band and nearly negligible for S-band at all times.

The attenuation results from the radiometric data apply to one-way semi-infinite path lengths in the direction of the antenna beams. The attenuation for finite path lengths can be determined from the above results by considering the geometry of any particular situation of interest.

A great advantage of the radiometric method of determining attenuation over the much more complex and costly method of monitoring beacons carried by probing rockets is that the transmission path and other experimental parameters can be easily controlled. For the purpose of obtaining attenuation data for more than one transmission path simultaneously, it would be highly desirable to utilize a multiple antenna-beam system in any future tests. Furthermore, the attenuation could be calculated more accurately and more often if additional microwave frequencies were employed. For these reasons, the following radiometric parameters are recommended for future tests.

<u>Microwave Frequencies.</u> L-, S-, X-, K_a-, and F-bands

<u>Antennas.</u> Parabolic with multiple feeds. Equal beamwidths for all frequencies would greatly simplify the interpretation of the data. A half-power beamwidth of about 1° would be a reasonable choice. Several of the beams should probe the fireball proper, and several of the beams should be aimed 10° to 20° away from the centers. A monopulse-type tracking of the fireball by the central antenna beams would be an attractive arrangement.

<u>Radiometers.</u> Conventional, comparison-type are desirable for the time interval from a few milliseconds to several minutes. For very early times, a simple directly connected radiometer should be developed.

<u>Recording.</u> Data reduction could be simplified immeasurably by converting the radiometer output from analog to digital form before processing. Strip-chart analog recording should also be retained to provide invaluable on-the-spot monitoring and diagnosis.

In the final analysis, the value of any experimental measurement must be judged by the extent to which it aids and encourages the invention and development of successful physical models and theories. In order that the resulting theories qualify as successful, they must predict reliably the outcome of hypothetical measurements over a wider range than the original measurements. The ultimate goal of the aggregate of electromagnetic measurements on the high-altitude nuclear bursts was to foster the formulation of a description of the time-space history of the elementary particles (including the radiation over the complete spectrum) involved in the burst with sufficient detail to permit the prediction of the electromagnetic blackout effects to be encountered in any foreseeable high-altitude nuclear threat. In this context, the results of the radiometric measurements were particularly rewarding. The time history of the emission temperatures and the transmission coefficients gave considerable insight into the physical processes.

The final results should prove to be of lasting value to both the theoretician and the radar systems engineer.

REFERENCES

1. R. B. Dyce, et al; "Riometer Measurements," P 374 ff, DASA Data Center Special Report 12, Proceedings; Debris Motion and Ionospheric Effects, February 1963; DASA Data Center, General Electric TEMPO, Santa Barbara, California; Secret Restricted Data.

2. L. Spitzer, "Physics of Fully Ionized Gas," Interscience Publishers, Inc., New York, 1956, P 65 ff; Unclassified.

3. R.H. Dicke, et al; Physical Review, Vol. 70, September 1946, P 340 ff; Unclassified.

4. DASA Data Center Special Report 7, Check Mate; DASA Data Center, General Electric TEMPO, Santa Barbara, California; Secret Restricted Data.

5. DASA Data Center Special Report 9, King Fish, November 1962; DASA Data Center, General Electric TEMPO, Santa Barbara, California; Secret Restricted Data.

6. U.S. Standard Atmosphere, 1962; NASA, USAF, USWB, U.S. Government, Washington, D.C., December 1962; Unclassified.

Pages 85-86 deleted.